Originally published as:

Yang, H., Wu, Z., Dawson, R. J., Barr, S., Ford, A., Li, Y. (2024): Quantifying surface urban heat island variations and patterns: Comparison of two cities in three-stage dynamic rural–urban transition. - Sustainable Cities and Society, 109, 105538.

DOI: https://doi.org/10.1016/j.scs.2024.105538

Quantifying surface urban heat island variations and patterns: comparison of two cities in three-stage dynamic rural–urban transition

Haibo Yang[a*], Zhengrong Wu[a], Richard J. Dawson[b,c*], Stuart Barr[b], Alistair Ford[b,c], Yunfei Li[d]

[a] School of Water Conservancy and Transportation, Zhengzhou University, Zhengzhou, CHINA

[b] School of Civil Engineering and Geosciences, Newcastle University, Newcastle upon Tyne, UK

[c] Tyndall Centre for Climate Change Research, Newcastle University, Newcastle-upon-Tyne NE1 7RU, United Kingdom

[d] Potsdam Institute for Climate Impact Research (PIK), Member of Leibniz Association, PO Box 60 12 03, Potsdam 14412, Germany

Corresponding author email: yanghb@zzu.edu.cn, richard.dawson@ncl.ac.uk

Graphical Abstracts

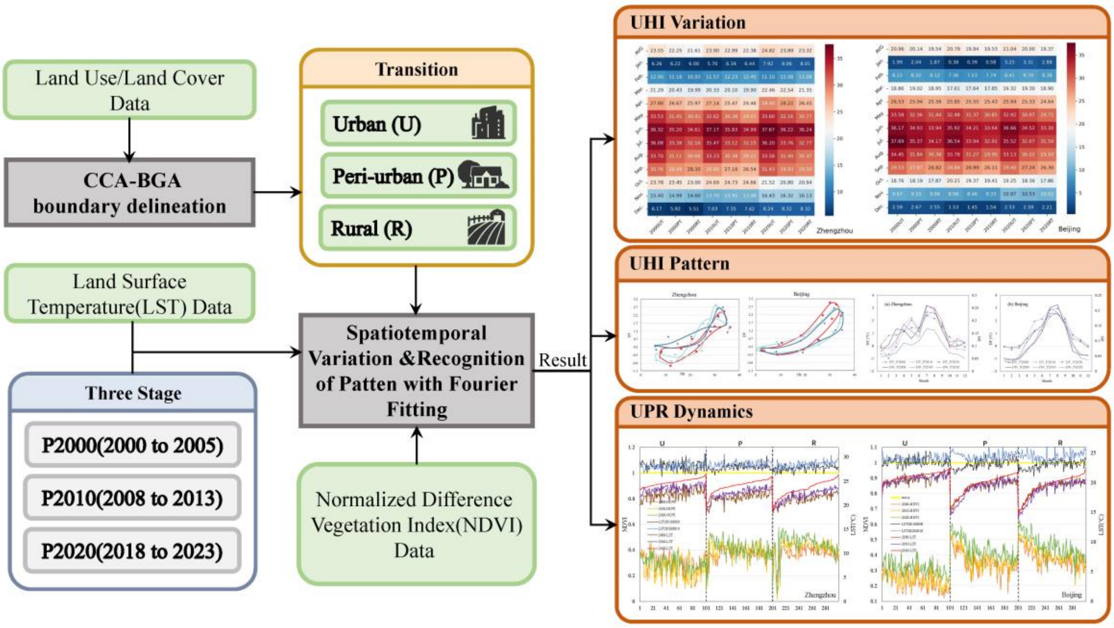

Highlights

- Spatiotemporal UHI variations response to dynamic rural-urban transitions.
- Three-stage analysis reveals long-term UHI and urbanization traits.
- UHI patterns differ in two cities based on surrounding crop cycles.
- The profiles in three stages show the horizontal and vertical expansion of the city

Abstract: Urban heat island (UHI) not only reflects the environmental thermal comfort and energy consumption, but also affects the urban meso-scale climate. There are many researches related with UHI mainly focusing on urban and rural area, while neglecting dynamic rural–urban transition especially in a rapid urbanization in China. Beijing and Zhengzhou are studied by using city clustering algorithm (CCA) and boundary generation algorithm (BGA) to delineate the urban, peri-urban and rural boundaries from 2000 to 2023 within three stages. Fourier transform model was used to identify the UHI patterns. Results show: 1) Two cities have undergone obvious expansions in 20 years, with a consistent mean LST decrease from urban to peri-urban and rural areas in three stages. 2) The distribution of UHII was more consistent in Beijing, while it varied more in Zhengzhou across seasons. 3) The UHI patterns notably differ, with Zhengzhou experiencing variable patterns and Beijing consistently showing oblate patterns. 4) The profiles of UHII and NDVI in two cities varied seasonally and reflected urban expansions in terms of longitude and latitude. Understanding the long-term changes and patterns of urban heat islands in different cities will provide information for formulating adaptive policies for urban sustainability.

Keywords: Urban heat island; Rapid urbanization; Urban expansion; MODIS; Remote sensing.

1 Introduction

Urban heat island (UHI), the temperature in urban area higher than that of in rural area(Oke et al., 2017), is one of the most reflection of human activities on natural environment. UHI not only represents apparently the temperature difference but also indicates energy balance difference which may affect the atmosphere-land-water cycle(Stassen et al., 2019), biodiversity(Knapp, 2010), even climatic change(Ghazanfari et al., 2009). The urban heat island phenomenon causes urban residents to live in discomfort, and in more extreme cases, it can lead to death(He, 2019; Hou et al., 2022; Kim and Brown, 2021). One research has shown that the heat island effect causes additional physiological stress in the human body, which may lead to the occurrence and aggravation of heat stroke, cardiovascular and respiratory diseases, especially in children and the elderly population(Shahmohamadi et al., 2011). Meanwhile, due to the high temperature in the city center, it has a negative impact on places that require cooling in summer, which means higher electricity expenditure for the country and is not conducive to environmental protection(Lu et al., 2010). Hence, the phenomenon of urban heat islands has garnered significant attention from urban planners, policymakers, environmental regulators, public health authorities, and the academic community.

From an internal perspective, the heat environment spatial distribution are inhomogeneous because of the different properties of urban and rural, including albedo and roughness of underlying surface(Li et al., 2021; Saaroni et al., 2018; Tian et al., 2021), energy consumption and emission(Ali et al., 2021), and sky-view factors caused by high-rise building(Dirksen, 2019).These urban characteristics differs from rural area by altering the natural surface energy and radiation balances (Oke, 1982). Meanwhile, activity-intensive areas in urban areas and a large number of buildings with high thermal mass and insulation may exacerbate the urban heat island effect (O'Malley et al., 2015). From an external perspective, global warming leads to an increase in average global temperatures, which increases heat in cooling-intensive areas such as urban areas and promotes the heat island effect(Kolokotroni et al., 2012).

According to the different measurement heights, research on urban heat islands is typically divided into canopy urban heat island (CUHI) and surface urban heat island (SUHI). CUHI is usually a small-scale and meticulous study, which typically employs measurement stations to obtain temperature data and calculate the UHI effect(Deilami et al., 2018), involves exploring detailed underlying surfaces and utilizing various statistical methods(Zou et al., 2021). However, the thermal environment typically exhibits clustered distribution and is influenced by the three-dimensional distribution of urban landscapes and buildings, as well as the spatial distribution of heat flux in the region. Small-scale analyses may not adequately reflect the overall situation, so remote sensing-based SUHI is widely employed in urban heat island research at the same time(Huang and Lu, 2018). In recent years, research that utilized large remote sensing datasets to study heat island patterns in 50 cities found that disparities in Land Surface

Temperature (LST) were evident not only between urban and natural categories but also within the urban categories(Bechtel et al., 2019a). Further research on the thermal conditions and driving factors of the urban interior three-dimensional landscape shows that, urban green space (UGI) and average building height (ABH) had a greater impact on SUHI intensity, with the relative contribution of UGI decreasing with the increase of building density and building height, while ABH showed the opposite trend(Zhou et al., 2022). Synthesizing current research, it can be found that due to its wide detection range and comprehensive spatial information, SUHI has been widely used in the study of urban heat issues and related urban heat island effects(Li et al., 2022; Xia et al., 2022; Zhou et al., 2018).

There are mainly two ways to differentiate the urban extent and background extent according to data used, city social-economic data and city spatial data. The method based on city social-economic data defines population agglomerations through Metropolitan Statistical Areas (MSAs), which start from a densely populated central area and include surrounding counties if there are social or economic connections. The method based on city spatial data involves generating Built-up Intensity (BI) maps through land use data to differentiate between cities and buffer zones with the same area as the cities(Zhou et al., 2014).

Although there are a lot of studies focusing on the UHI dynamics and some critical questions are still not emphasized. (1) Urban heat island patterns are usually studied by geographically weighted regression(Gao et al., 2022), Geodetector(Feng et al., 2021), random forests(Oukawa et al., 2022) and other methods. Although these methods can better handle a large number of variables, they have a lower degree of visualization and cannot better respond to the changing pattern of urban heat island between multiple time periods. (2)UHI or Land Surface Temperature(LST) studies based on single time-point and a continue time-series data (Busato et al., 2014; Geng et al., 2023; Li et al., 2011) have different usage and reliability. Opting for the mean value of continuous time series alone may result in a weakened representation of the urban heat island phenomenon during calculation. Moreover, geophysical and climatic phenomena often lack specificity when based solely on results from a singular point in space or time. (3)The boundary of urban and rural is the critical factor influencing the UHI results(Azevedo et al., 2016). Numerous studies(Bechtel et al., 2019b) have attempted to clarify the impact of spatial and temporal variation on the urban heat island phenomenon and the spatial pattern on the thermal environment in urban areas through the temperature difference between the city and the suburbs, however, many current studies do not take into account the existence of buffer zones between urban and rural areas.

Given the three issues identified in urban heat island research and the rapidly deteriorating environmental hazards caused by the heat island effect, there is an urgent need for a more comprehensive approach to quantifying changes and patterns in the surface urban heat island, providing city planners and governments with accurate quantitative methods and a basis for action. Therefore, this paper starts from multiple dimensions across different times and spaces, analyzing the changes in the heat island distribution of two cities representing different levels of development in China over the past 20 years: Beijing and Zhengzhou. Specifically, the goal of this study is: (1) Reveal the differences in heat island patterns brought about by urban-rural changes. (2) Propose methods to address the weaknesses in representation of the UHII when relying solely on mean values or data from singular points in space or time. (3) Propose an extended solution aimed at addressing a oversight in traditional urban heat island effect calculations: the insufficient consideration of buffer zones between urban and rural areas.

2 Data and Methods

2.1 Study area

Beijing, a great mega-city in the world, has experienced rapid growth, with population escalating from 13.636 million in 2000 to 21.843 million by the end of 2022. The urbanization rate of Beijing rose from 54.9 percent in 1978 to 85.9 percent in 2018, and is now at an advanced stage of stable urbanization(Dai et al., 2022). Beijing, serving as China's capital and political center, has rapidly evolved into a global first-tier city, encapsulating the developmental characteristics of great mega-cities in China. Zhengzhou is a megacity, currently defined as a second-tier city by the Chinese government, located in the central and northern region of China, serving as the capital of Henan Province. In the past two decades, Zhengzhou has witnessed significant economic growth, experiencing rapid urbanization. Zhengzhou, as a typical city benefiting from China's policy of prioritizing the development of provincial capitals, is the fastest-growing city in the province. Beijing and Zhengzhou are representative of two types of cities in China—first-tier and second-tier cities, respectively. Therefore, we have selected Beijing and Zhengzhou as the subjects of our study for comparative analysis, aiming to explore the SUHII (Surface Urban Heat Island Intensity) response under varying urban expansion rates.

2.2 Data sources and pre-processing

Globe Land Collection 30 (GLC30) developed by the National Geomatics Center of China, with an overall spatial accuracy of 82.4% and a spatial resolution of 30m in China is used to better extract built-up areas(Jun et al., 2014). This data was classified for land cover using interactive human-computer methods, based on multispectral imagery from the United States' Landsat satellites (TM5, ETM+, OLI) and China's HJ-1 environmental disaster mitigation satellite. It has high spatial accuracy in China and has been widely used by scholars for calculating relevant indices in urban heat island assessments as underlying surface data(Cai et al., 2023; Li et al., 2024; Yan et al., 2022). GLC30 is distributed through the website provided by the National Geomatics Center of China (http://globeland30.org). GLC30 presentations for the three periods can be found in Fig.1. MOD11A2, with a 500m resolution, provides an 8-day combination of MODIS land surface temperature products. Each pixel value in MOD11A2 is a simple average of all the corresponding MOD11A1 LST pixels collected during that 8-day period. MOD13A2 provides Normalized Differential Vegetation Index (NDVI) values per pixel at 1 km spatial resolution. The algorithm of product selects the best available pixel value (low cloud, low view Angle) from all the acquisition over a 16-day period. The derived products of MODIS have a higher temporal resolution, thus they can reflect the fine-grained changes in heat islands. This product is also widely used by scholars for the research of heat islands(Clinton and Gong, 2013; Liao et al., 2022; Mohammad and Goswami, 2023) .MOD11A2 and MOD13A2 are distributed by the Level-1 and Atmosphere Archive and Distribution System (LAADS) and are available through the website (https://ladsweb.modaps.eosdis.nasa.gov) .

Compared to land, water bodies have a higher specific heat capacity, which makes them heating slower during the day and cooling slower at night. This physical property causes a significant temperature difference between the water body and the surrounding surface, which affects the accuracy of UHI calculation. Therefore, in this study, LST pixels in the water body area were removed to improve the accuracy of SUHI evaluation.

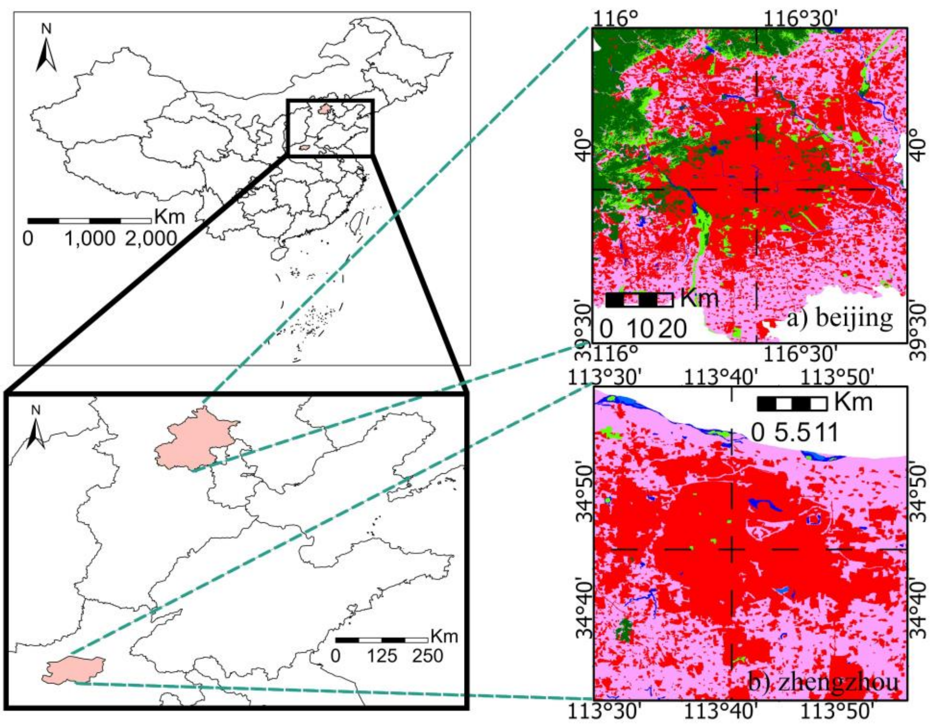

Fig. 1. The land use/land cover (LULC) of GLC30 in the study area. The red area is artificial land, the pink area is cultivated land, the blue part is water, and the green part is woodland or grassland. The black dashed line represents the vertical and

horizontal lines starting from the center point of the minimum bounding rectangle in the urban impermeable area. This line is the contour line mentioned later

In addition, we utilized ERA5-Land, a reanalysis dataset that offers a coherent perspective on the changes in meteorological parameters over multiple decades. This dataset provides temperature data at a finer resolution than ERA5, enabling us to extract a more detailed view of temperature trends. Compared with the point data of traditional weather stations, the per-pixel data provided by the ERA5-Land is more fine-grained. It provides air temperature 2 meters above the surface of land, sea or inland water, within urban areas inhabited by humans, offers a more accurate reflection of the effects of urban heat island on human life.

2.3 The urban and rural extent delineation

To better research the response of two different levels of urban sprawl to the urban heat island phenomenon, 30m resolution land cover data (GLC30) of 2000, 2010, and 2020 are divided into three areas of equal area: city urban (U), peri-urban (P), and rural (R) by using CCA and BGA. Due to the fact that the error in selecting the average value of a continuous time series alone is greater than that of a long time period, we divided the imaging cycle of GLC30 products into three time periods: P2000 (2000.3 to 2005.2), P2010 (2008.3 to 2013.2), and P2020 (2018.3 to 2023.2). And then, all temperature of cluster (TC), temperature of background (TB), UHII and Temperature Difference (DT, means temperature of the cluster minus the temperature of the background) are calculated in three periods: P2000, P2010 and P2020.

2.4 Identification of UHI patterns using Fourier transform models

To disclose the UHII change response to urban expansion due to rapid urbanization, third order Fourier series transformation model was chosen to build the UHI patterns, from which TB-DT relationship is interpreted. The formula is shown as Equation 1:

$$F(t) = a_0 + \sum_{n=1}^{3}\left(a_n \cos\frac{2\pi nt}{P} + b_n \sin\frac{2\pi nt}{P}\right) \quad (1)$$

where $F(t)$ means either TB or DT, P represents 12 months, t the times $t; t = 1,2 \dots 60$, a_0, a_n, b_n are the Fourier coefficients, a_0 is especially referred to as the mean of $F(t)$. After the coefficients are obtained, fitted values of TB_i and DT_i are used to build the fitting curve.

Since peri-urban and rural areas have more similar characteristics, we consider combining the two on the calculation of the traditional UHII. UHII is calculated by the following formula:

$$UHII^{(p)} = T^{(p)} - \frac{\sum_{i=1}^{n} T_p^{(i)} + \sum_{j=1}^{m} T_r^{(j)}}{n+m} \quad (2)$$

where $UHII^{(p)}$ is the UHII of p-th pixel, $T^{(p)}$ means the temperature of p-th pixel, n and m refer to total pixels of peri-urban and urban. $T_p^{(i)}$, $T_r^{(j)}$ is the temperature value of the i-th, j-th pixel in the peri-urban, rural region, respectively.

The method for UHI pattern recognition based on Fourier fitting is illustrated in Fig 2. Initially, we acquire the LST layer from MOD11A2, followed by extracting the LST layer for areas determined by the CCA-BGA algorithm. Subsequently, we calculate the DT (UHII) and determine the monthly averages for TB and DT. A Fourier fitting relationship between TB and DT is then established. Finally, we create graphs and conduct analysis based on this relationship.

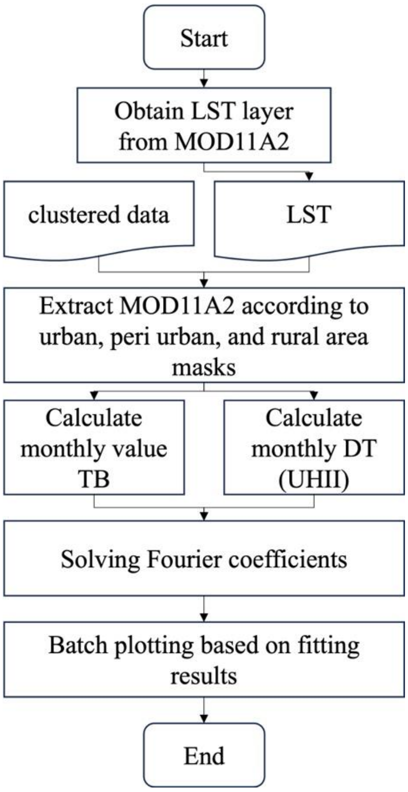

Fig. 2. Flowchart of the UHI Pattern Recognition Process.

3 Results

3.1 Three stages rural–urban dynamic transition

Table 1 and Fig. 3, the average area of Zhengzhou increased by 2.20 times from 2000 to 2010, 2.05 times from 2010 to 2020. The average area of Beijing increased by 1.42 times from 2000 to 2010, 1.53 times from 2010 to 2020. The cluster area of Zhengzhou in 2020 is roughly the same as that of Beijing in 2000.

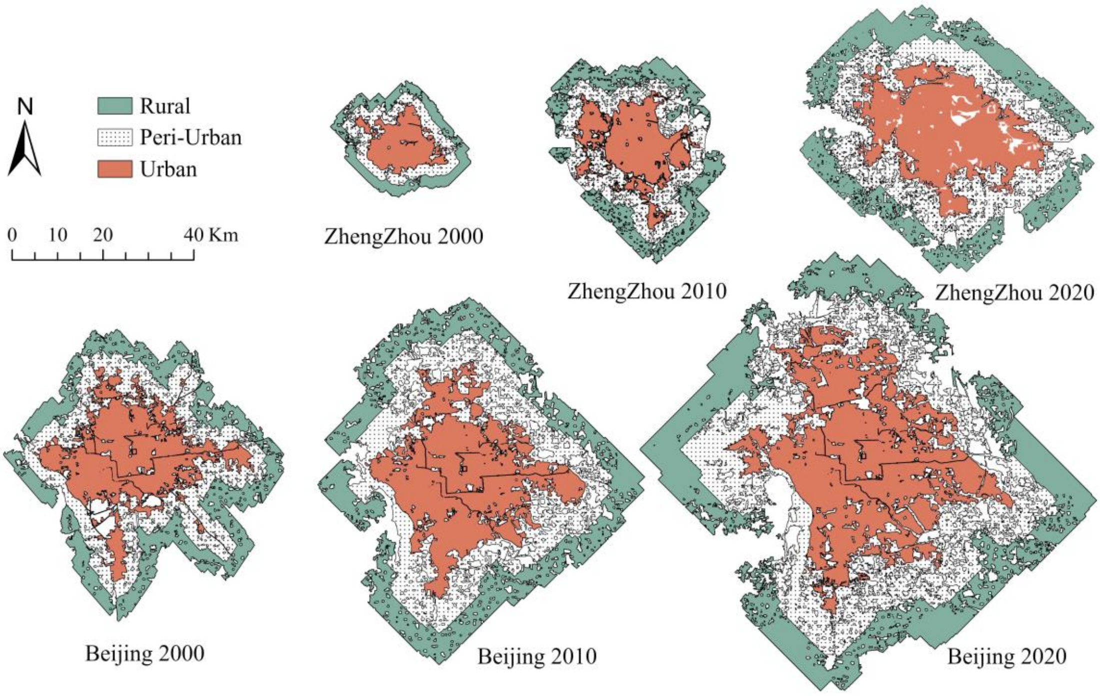

Fig. 3. The cluster map and boundary map of Zhengzhou and Beijing

Table 1. Cluster area of Beijing Zhengzhou, 2000,2010, and 2020

Area (km^2)	2000			2010			2020		
	U	P	R	U	P	R	U	P	R
Beijing	652.68	653.38	651.84	925.49	924.44	925.97	1419.98	1418.74	1421.16
Zhengzhou	153.97	153.56	154.50	338.62	338.84	339.50	693.19	693.40	694.30

It can be seen from the average monthly LST data (Fig. 4) that urban, peri-urban and rural areas of Zhengzhou have the highest mean LST values in June, which is increasing every year (36.32°C, 37.17°C, 37.67°C), while the highest temperature in Beijing in each study period was distributed in different months. In P2000 and P2010, the highest temperature of Beijing was in July (37.69°C, 36.54°C), but in P2020, it was in June(36.66°C). The majority of the high-temperature period (most are above 25°C) is concentrated between April and September in Zhengzhou and Beijing, while the moderate-temperature period (most are between 15°C and 25°C) is concentrated in March and October and the low-temperature period (most are below 15°C) is concentrated in January, February, November and December. In most months in

Zhengzhou, the average LST of U, P and R decreased, except for January, February, November and December P2010, which increased in February P2020, October P2010, January P2020, March increased first and then decreased, and June P2020, October decreased first and then increased. In most months in Zhengzhou, the average LSTs of U, P, and R decrease, except for January, February, November, and December of P2010, and February of P2020, where they increase. In October of P2010 and January, March and December of P2020, they increase first and then decrease. In June and October of P2020, they decrease first and then increase. In most months in Beijing, the average LSTs of U, P, and R also decrease, except for January and February of P2010, where they increase. In January, February, March, and December of P2000, and January, February, and December of P2020, they increase first and then decrease. In October and December of P2010, they decrease first and then increase. In both Zhengzhou and Beijing, the mean values from U to P and from P to R decrease in each period. In Zhengzhou, from U to P and from P to U, they decrease by 1.13°C and 0.61°C in P2000, 0.84°C and 0.41°C in 2010, 0.76°C and 0.48°C in P2020. In Beijing, from U to P and from P to U, they decrease by 0.82°C and 0.6°C in P2000, 0.95°C and 0.31°C in 2010, 1.04°C and 0.63°C in P2020.

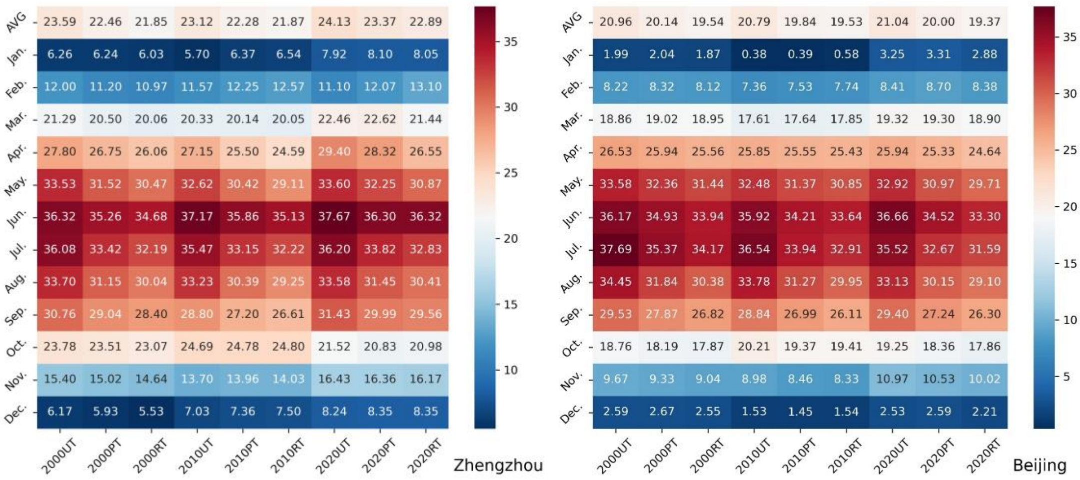

Fig. 4.Mean monthly LST of two periods in urban, peri-urban and rural of Beijing and Zhengzhou. The abscissa represents the temperature of the region (U, P, R) in three stages. The ordinate is an acronym for the month, while the first row is the average for the corresponding region and time period.

As shown in Fig. 5, for all the points, the average surface temperature ratio (P2010/P2000) for the first 10 years and the average surface temperature ratio (P2020/P2010) for the next 10 years in Zhengzhou are 1.055 and 1.053, respectively. In Beijing, they are 1.006 and 1.023, respectively. It can be observed that both cities are experiencing warming trends internally. Similarly, the surface temperature ratios for the P region and R region in the last 10 years are higher than those for the previous 10 years, and this trend is also observed in Beijing. The difference lies in the fact that in the first 10 years, only 49% of the points in Beijing had surface temperature ratios more than 1, indicating that less than half of the points experienced a increase in surface temperature. However, in the second 10 years, 84% of the points had surface temperature ratios greater than 1. In Zhengzhou, these two ratios are closer, reaching 91% (P2010/P2000) and 98% (P2020/P2010) respectively, indicating a uniform increase in surface temperature within the region. In all three time periods, NDVI values in all areas of Beijing increased over time, while in Zhengzhou's U region, they initially decreased and then increased. Beijing's NDVI experienced rapid growth from P2000 to P2010. At any given time, the NDVI distribution in the U area is always lower than in the P area, which in turn is consistently lower than in the R area. In the three time periods, surface temperatures within the urban area of Zhengzhou exhibited a more pronounced increase, measuring 22.294, 23.488, and 24.721°C, respectively. Surface temperatures in the U, P, and R regions also showed a slight upward trend. This phenomenon is not obvious in Beijing, where the surface temperature profiles for the three time periods in the U-region are closer, with mean values of 20.544, 20.629 and 21.086°C, respectively. Furthermore, surface temperature fluctuations in Beijing's P and R regions are greater than those in Zhengzhou, which may be attributed to the more intensive urbanization and construction activities in Beijing's P and R regions.

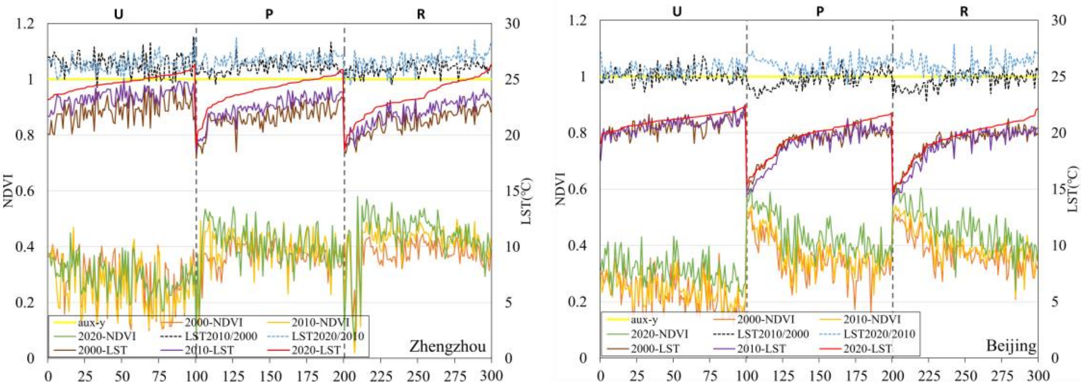

Fig. 5. 100 random points were generated on each of the three regions U, P, and R and the average value at the point was extracted. The random points were sorted in ascending order according to the LST of P2020. The random points within the U, P, and R regions were labeled from 1 to 100, 101 to 200, and 201 to 300, respectively,

according to the sorted order. The dashed line in the figure indicates the LST ratio of the two time periods. The coordinate axis on the left is the shared axis for the ratio of NDVI and LST. The coordinate axis on the right is LST.

3.2 UHII spatial and temporal variation

As stated in Fig. 6, the overall changes in the means of the two cities are relatively regular. The annual mean values of UHII in Zhengzhou were 1.474, 1.107, and 1.046, respectively, and experienced a continuous decline, whereas the annual mean values in Beijing declined and then increased, and were very close to each other at P2000 and P2010, reaching 1.126, 1.114, and 1.529 in the three time periods, respectively. the mean values of UHII in spring in Zhengzhou were higher than those in autumn, whereas the opposite was the case in Beijing.

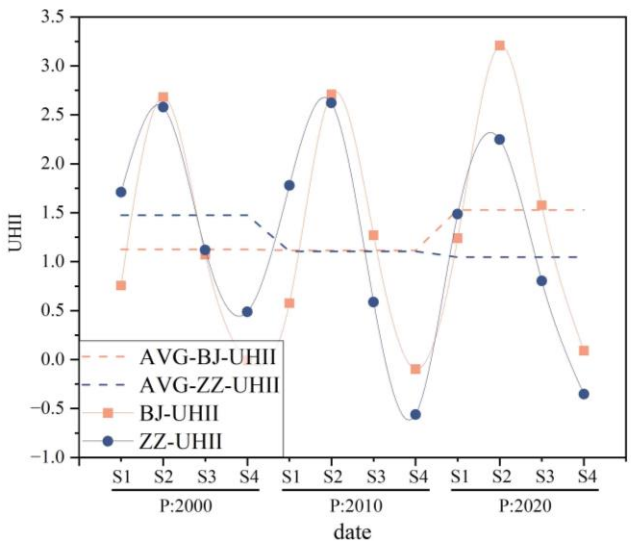

Fig. 6. Annual UHII and quarterly UHII transformations for both cities. S1, S2, S3 and S4 represent spring, summer, autumn and winter.

As illustrated in Fig. 7, the overall UHII distribution in Beijing is relatively stable, while Zhengzhou shows a large variation in all seasons. The UHII mean values for all years in the inner-city summer in Zhengzhou were 2.483 and 2.867 for Beijing, respectively, indicating that the heat island intensity in Beijing was higher than that in Zhengzhou during this summer. The mean value of UHII in winter in Zhengzhou is -0.142, while the mean value of UHII in Beijing cluster area is -0.005, which indicates that the urban cold island phenomenon in winter is more prominent in Zhengzhou than in Beijing. It is worth noting that the UHII value within the city of Zhengzhou in spring is 1.658, which is significantly higher than 0.858 in Beijing. The presence of a heat island effect in Zhengzhou was apparent across all four seasons in the 2000 period. Specifically, the heat island phenomenon was more prominent during spring, summer and winter of that year. In Beijing 2000 period, the urban areas with temperatures lower than the background in spring and winter accounted for 0.489 and 0.504 of the total urban area, respectively, and the heat island was more obvious in summer. In the 2010 period of Zhengzhou, the heat island in spring and summer was evident, which gradually dissipated during autumn, and cold island appeared in winter. In the same time period, the heat island in summer and autumn was obvious in Beijing. During the spring of 2020 period, no significant heat island effect was observed in Zhengzhou, while cold island effect was observed in winter. In the summer season, the UHII in the city center is concentrated, while in the autumn season, the heat is transferred to the east. In the 2020 period, the distribution of UHII in summer and autumn is similar in Beijing, with higher UHII values in the southern part and lower values in the northern part in the spring and winter seasons.

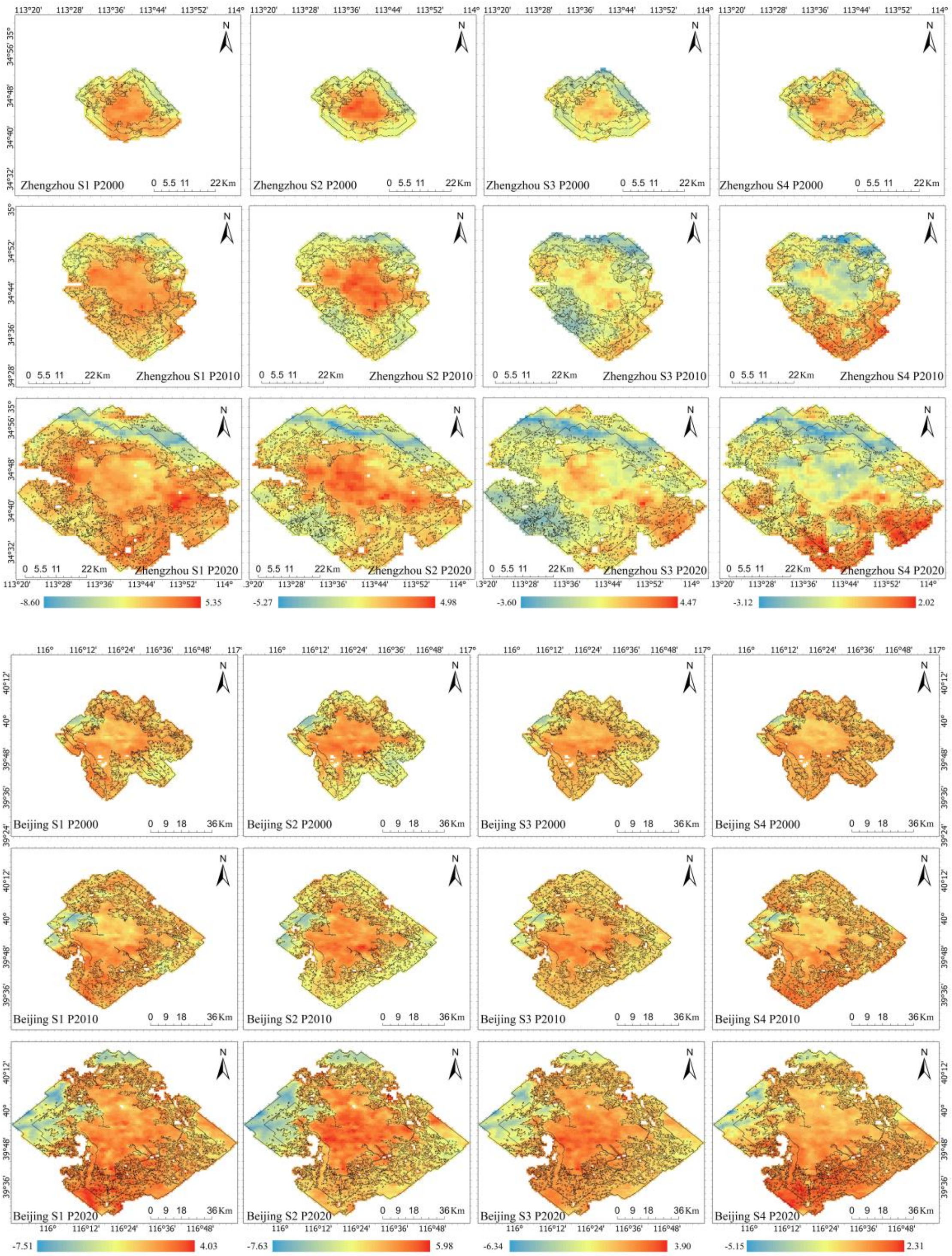

Fig. 7. Spatial and temporal distribution of UHII. The legend of each row is represented by the color bar located on its right-hand side. S1, S2, S3, and S4 represent spring, summer, autumn, and winter, respectively. P2000, P2010, P2020 refers to the period from 2000 to 2005, 2008 to 2013, and 2018 to 2023.

3.3 Intra-annual UHI patterns

Smooth curves are used to connect the Fourier transform results as shown in Fig. 8. It can be seen that the Fourier fitting curve of Zhengzhou is spiral in 2000 and 2010 periods, and oblate in 2020 period, while Beijing is oblate in all periods. The transformation of Zhengzhou in 2020 period can be explained by the higher UHII observed after September as compared to the period between January and April. This led to a counterclockwise curve in 2020 period, which is significantly different from the complex patterns observed in 2000 and 2010 periods, and bring the city closer in line with Beijing in the shape of the curve, where three similarly shaped curves were observed at different time periods. The general fitting curves of Beijing during the time periods of 2000, 2010, and 2020 show an upward trend, indicating the rise of UHI effect in tandem with urban expansion. But this situation is not suitable for Zhengzhou because the curve of Zhengzhou illustrates a complicated trends, especially in 2000 period, the UHII of January, February, March and April in 2000 period was higher than that of October, November and December, in 2010, the UHII of November and December is larger than that of January and February, and that of March and April is larger than that of September and October, August and July are larger than that of May and June, in 2020 period, July, August, September, October, November, and December are larger than January, February, March, April, May, and June. From a trend perspective, the pattern in Zhengzhou is gradually converging with that of Beijing, reflecting an upward regularity in the urban heat island phenomenon as temperatures rise. We speculate that this shift may be associated with the policies and geographical positions of the two locations.

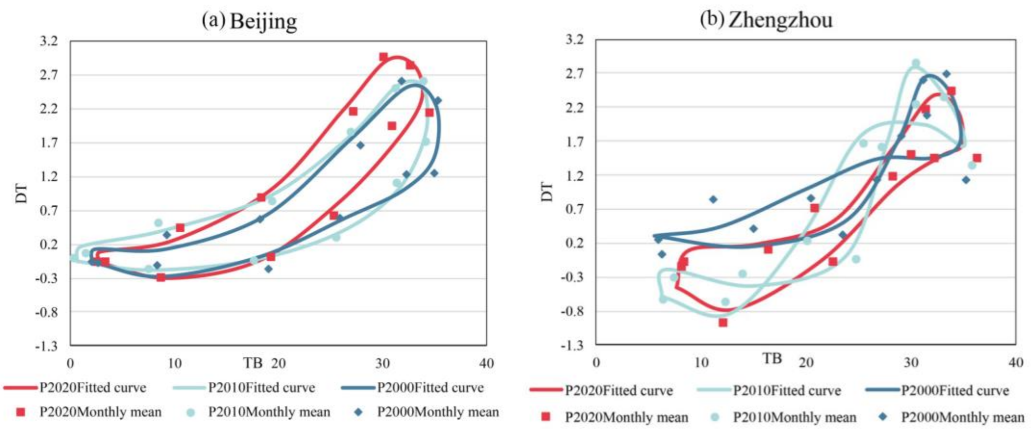

Fig. 8. Combination characteristic curve of fitted UHI and monthly mean value. (a) Beijing, (b) Zhengzhou. The fitted closed curves are obtained from the Fourier transformation, the delta points are the monthly mean value of DT.

In Zhengzhou, the DN-DT curves (Fig. 9) show a bimodal shape and the peak values of them are: 2.08°C (May) and 2.69°C (July), 2.24°C(May) and 2.85°C(August), 1.15°C (May) and 2.44°C (July) in 2000, 2010 and 2020 periods. This does not apply to Beijing, while there was a unimodal shape in Beijing, which was 2.61°C(August), 2.61°C (July), 2.97 °C(August) in the same times. Similarly, we observe that Zhengzhou has a bimodal DN curve with peak values of 0.167 (March) and 0.260 (July), 0.184 (April) and 0.257 (July), 0.112 (April) and 0.168 (July), while Beijing still corresponds to a unimodal DN curve with peak values of 0.219 (August), 0.209 (July), and 0.191 (August). This phenomenon suggests a potential relationship between the monthly distribution of NDVI and UHII. Moreover, the minor peaks of DN in Zhengzhou always occur before UHII, while the peaks of DN in Beijing always occur simultaneously with UHII, and the slopes of DN and UHII in Beijing during three periods are similar from June to October, which are the same as in Zhengzhou.

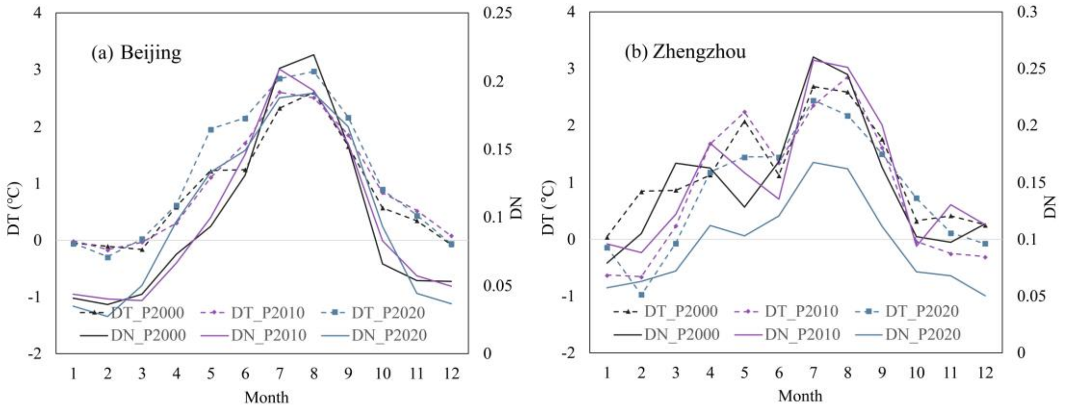

Fig. 9. The mean monthly different temperature (DT, defined as the average temperature in clustered zones minus the average temperature in boundary zones) and different NDVI(DN, defined as the average NDVI in clustered zones minus the average NDVI in boundary zones) in three periods (P2000, P2010 and P2020) in Beijing (a) and Zhengzhou (b).

3.4 Profiles of UHII and NDVI

Fig. 10 shows yearly UHII and NDVI cross profile in three stages in Beijing and Zhengzhou. We can see the strong negative relation between UHII and NDVI. It is noteworthy that the expansion of a city does not necessarily lead to NDVI decrease in the internal and external of city. The NDVI of the urban area of Beijing showed an increasing trend in these three time periods, but there was no specific trend in the suburbs. This may be related to the urban greening measures implemented in Beijing. However, this cannot be used to explain Zhengzhou, which had the lowest NDVI in 2010 and the highest NDVI in 2020 period in the horizontal direction of urban center. From a temperature perspective, both Beijing and Zhengzhou exhibit a north-south temperature gradient. Vertically, Beijing shows higher temperatures in the central region and lower temperatures on both sides, with the eastern side being higher than the western side. In Zhengzhou, the temperature remains higher in the central region horizontally, but there is no consistent rule in the temperature variations of the suburban areas on the eastern and western sides. This can be attributed, to some extent, to the changing expansion directions of Zhengzhou.

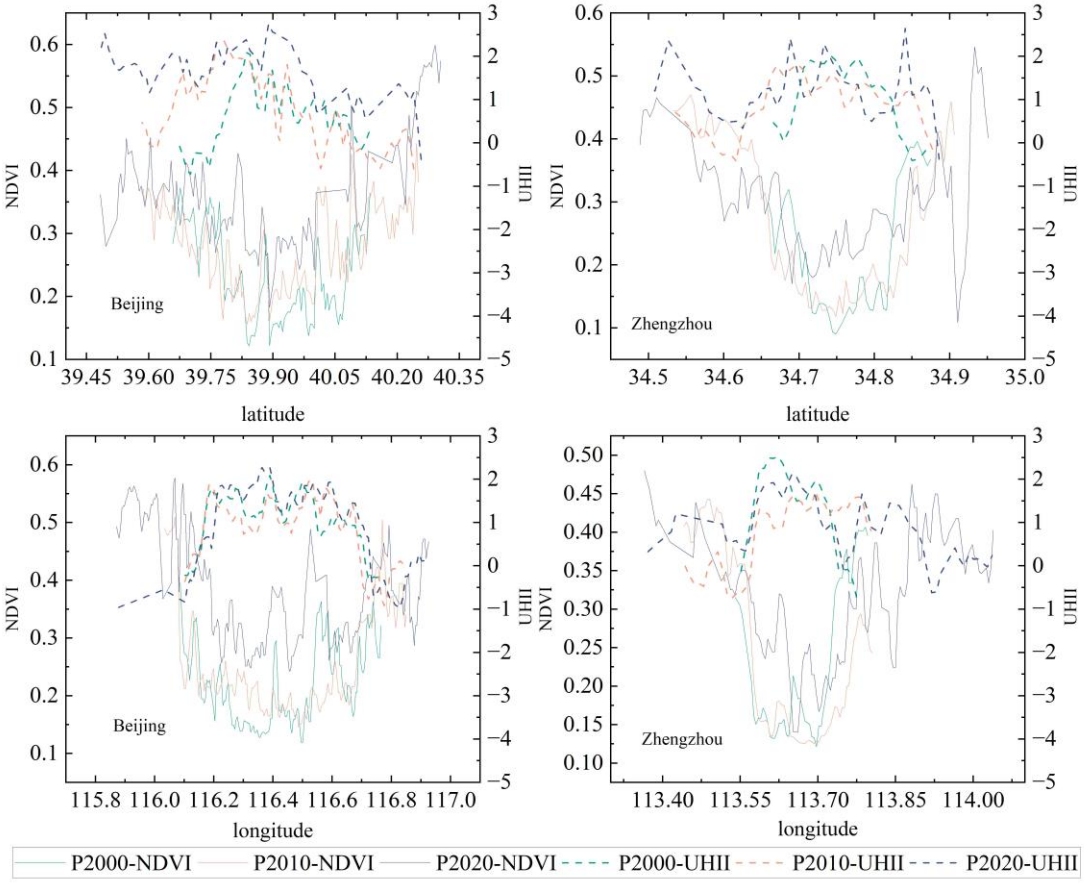

Fig. 10. Aggregate yearly UHII and NDVI profile in three stages in Beijing and Zhengzhou.

Two cities profiles of UHII and NDVI show slight variations across different seasons in Fig. 11. The UHII distribution in Zhengzhou in summer is high in the middle and low on both sides in each period, whether horizontal or vertical. In the vertical direction, the UHII in Zhengzhou is high in the south and low in the north at all time periods. During the 2010 period, the winter UHII in the central urban area of Zhengzhou was lower than that in the surrounding area, until 2020 period, a multi-peak situation was formed, and the regional distribution of the same latitude was inherited. In the vertical profile of Beijing in 2000 period, the UHII distribution in winter is very different from that in spring, summer and autumn. In the vertical profile of Beijing in 2000 period, the UHII distribution in winter is very different from that in spring, summer and autumn. Winter UHII is high in the south and low in the north, while the other seasons are the highest in the middle. In the vertical profile of Beijing in 2000 period, the UHII distribution in winter is very different from that in spring, summer, and autumn, with winter UHII being high in the south and low in the north, while the other seasons are the highest in the middle. This rule does not apply to 2010 and 2020 period, as in these two years, the UHII in the southern suburbs was higher than that in the north. Similarly, in the vicinity of the same location, the UHII distributions for each season are relatively similar.From the horizontal direction, similar to the vertical direction, the UHII distribution in Zhengzhou in the winter of 2010 period is different from that in other seasons. The UHII distribution in the suburban areas shows significant variations across different seasons. During the 2000 period, UHII were higher in the western region compared to the eastern region. However, in the 2010 period, the situation reversed, with UHII being higher in the eastern region compared to the western region. By the 2020 period, the peak UHII shifted westward, while still maintaining its location from the 2010 period. This indicates that urban development during the 2020 period has been gradually considering the optimization of the urban heat environment. Over the periods, the UHII difference during Beijing's summer has been increasing, while the UHII range showed a reduction in 2010 period during the winter. Beijing exhibits a noticeable UHII distribution in the horizontal profile, with higher UHII in the central region and lower UHII on both sides. In the suburban areas, there is a consistent trend of lower UHII in the western region compared to the eastern region throughout the year, which might be attributed to the presence of mountainous areas in the western part of Beijing. Consistent with Zhengzhou, during the 2010 period, the horizontal UHII distribution in Beijing's winter still showed some inconsistencies compared to other seasons. To get the heat island expansion size, we further calculated the peak length transformations in the figure, where Beijing, in the longitudinal direction, ranges from 9.99 to 28.97 to 44.95 km; and Zhengzhou from 10.99 to 19.98 to 18.98 km. Horizontally, Beijing goes from 32.96 to 33.72 to 43.69 km; Zhengzhou goes from 13.95 to 18.06 to 23.80 km. This finding indicates that the heat island area in Beijing has expanded in both directions, while Zhengzhou experienced a contraction in 2010, which aligns with earlier conclusions.

When comparing the mean NDVI values of Zhengzhou and Beijing for each time period, we found that the mean NDVI values of Beijing were lower than those of Zhengzhou in spring, but higher than those of Zhengzhou in summer and autumn; in winter, they were similar to those of Zhengzhou. This difference stems from the differences in crop types and phenology between the two places. In order to gain a deeper understanding of the differences between NDVI within the city and the surrounding areas, we performed K-Means clustering on the profile data in each season, setting the number of clusters to 3 and the maximum number of iterations to 1000 based on the UHII profile analysis above. The synthesis revealed that the differences in NDVI between Beijing and Zhengzhou were manifested in the seasonal variability, the orientation variability, the temporal variability, and the longitudinal and transverse variability, and the rule of variation is almost opposite to that of UHII. The longitudinal data showed that the mean NDVI values of Beijing in all seasons increased year by year. This suggests that, in spring in Beijing NDVI difference with the eastern periphery increased significantly at P2020, while the difference with the western periphery was relatively stable. In summer, the difference with the eastern periphery increased significantly at P2020, and the difference with the western periphery decreased slightly after peaking at P2010. In autumn, the difference with the western periphery is negative at P2010, which means that the NDVI values within the city are lower than its western periphery. The difference with the eastern perimeter is relatively stable. In winter, the difference with the western periphery is negative at P2020, while the difference with the eastern periphery gradually approaches zero. This law is just in conflict with the UHII calculation. The cross-sectional data show that the NDVI values in Beijing are very similar vertically and horizontally in spring, autumn, and winter, with a difference of only 0.02 in summer. By calculating the difference between the mean value of the inner-city areas and the outer areas over three time periods, we found that in spring, the differences with the southern perimeter increased sharply and then declined gently over time, and the differences with the northern perimeter stayed in a downward trend with an increasing rate of decline, which may be related to the fact that vegetation in the northern countryside grew faster in the spring relative to the southern perimeter. By summer, the difference in NDVI with the southern perimeter over time was exactly the opposite of the spring trend. By autumn, the trends in NDVI differences with the northern and southern perimeter were closer together. In winter, the NDVI difference with the southern periphery was increasing, and the NDVI difference with the northern periphery was decreasing and then increasing. Similar to Beijing, the mean NDVI in Zhengzhou also increases year by year. The K-means clustering results indicate that in all seasons, the differences between Zhengzhou and the western The NDVI difference between Zhengzhou and the western periphery was generally large, especially in summer when it reached a maximum value of 0.350. For the difference with the western periphery, the NDVI differences between P2000 and P2010 were similar in spring. For the differences with the eastern periphery, the trends of P2000 and P2010 in spring, summer, autumn and winter are similar. Zhengzhou's NDVI values in all seasons have very similar vertical and horizontal means in the three periods. The trends of NDVI differences in the three time periods were generally consistent according to the results of K-means algorithm. In spring and autumn, the difference with the southern periphery is larger.

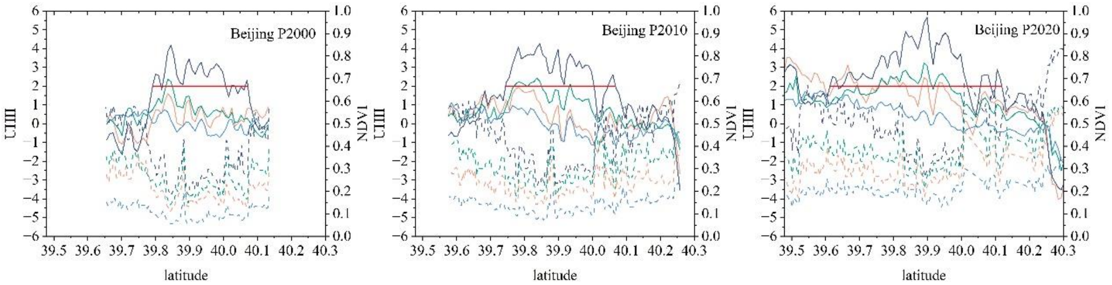

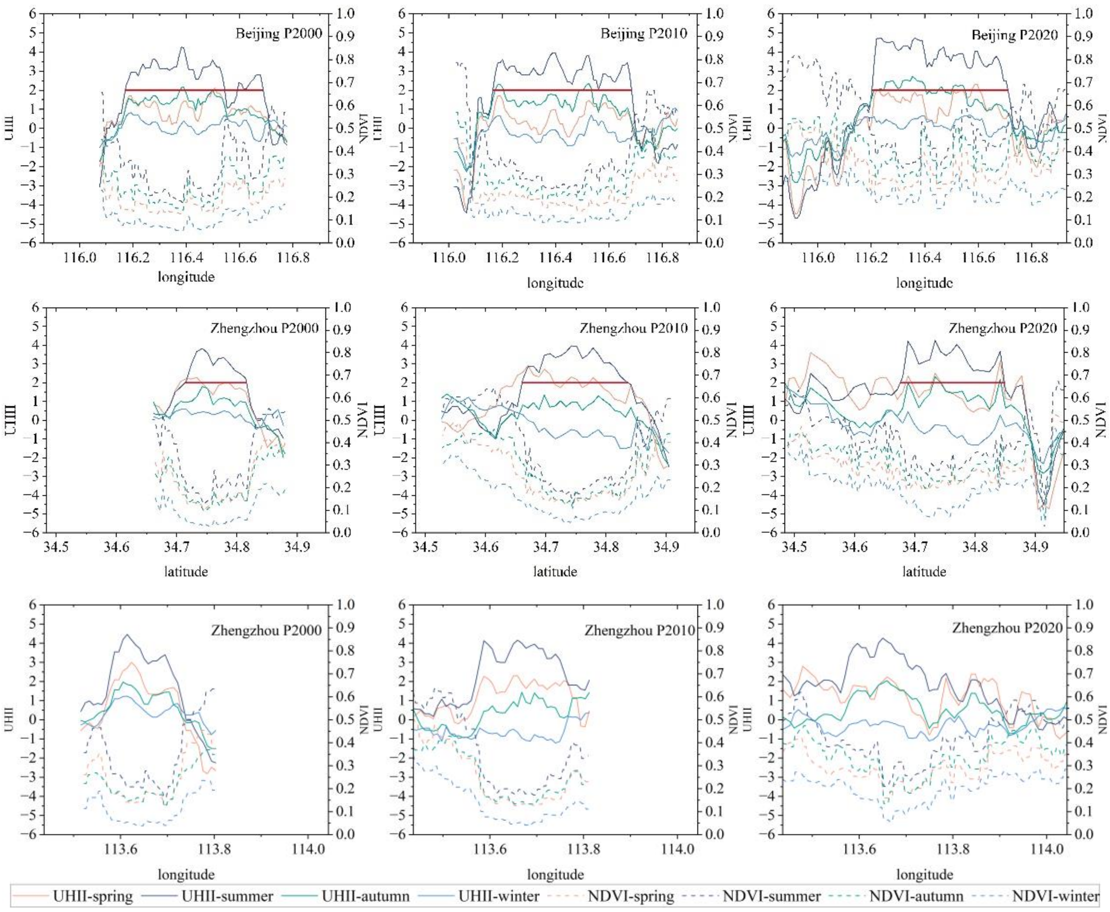

Fig. 11. Synthesized seasonal UHII and NDVI profiles from Zhengzhou and Beijing mean values. The red line represents the segment cut by the summer UHII curve when UHII equals 2. This segment can represent the span of the heat island in two directions.

3.5 LST and Air temperature comparison

It is generally assumed that there is a significant correlation between air temperature and LST(Mutiibwa et al., 2015). The absorption of solar radiation by the atmosphere and the ground increases the temperature of the atmosphere and the land surface(Lacis and Hansen, 1974). We calculated and obtained quarterly trends in average urban, peri-urban and rural surface temperatures and urban air temperatures as shown in Appendix A. The surface temperature is usually higher than the air temperature, especially on the ground that receives direct solar radiation, while the air absorbs the long-wave radiation emitted by the ground. The atmosphere exchanges energy with the surface through processes such as convection, evaporation, transpiration, and heat conduction. We first attempted to explore the overall period fitting relationship between atmospheric temperature and LST. As shown in Fig. 12, the coefficient of determination for Zhengzhou in urban, peri-urban, and rural areas is 0.8676, 0.8509, and 0.8537, respectively, while for Beijing, it is 0.9046, 0.8903, and 0.8833. It can be seen that both Zhengzhou and Beijing have better fitting effect and linear relationship.

However, when we fit the data using quarterly mean values (Fig. 13), we found that the coefficient of determination for both Zhengzhou and Beijing are lower than that for the overall. In Zhengzhou, the four seasons of the coefficient of determination were 0.3345, 0.4565, 0.2724, 0.5677, in Beijing, 0.6828, 0.4357, 0.5088, 0.7588. This suggests that the relationship in air temperature and urban land surface temperature varies greatly across seasons and may not exhibit a significant linear relationship between different cities, while the overall trend indicates a significant linear correlation between the two variables. Hence, it is crucial to perform analyses of urban heat islands across different seasons in cities.

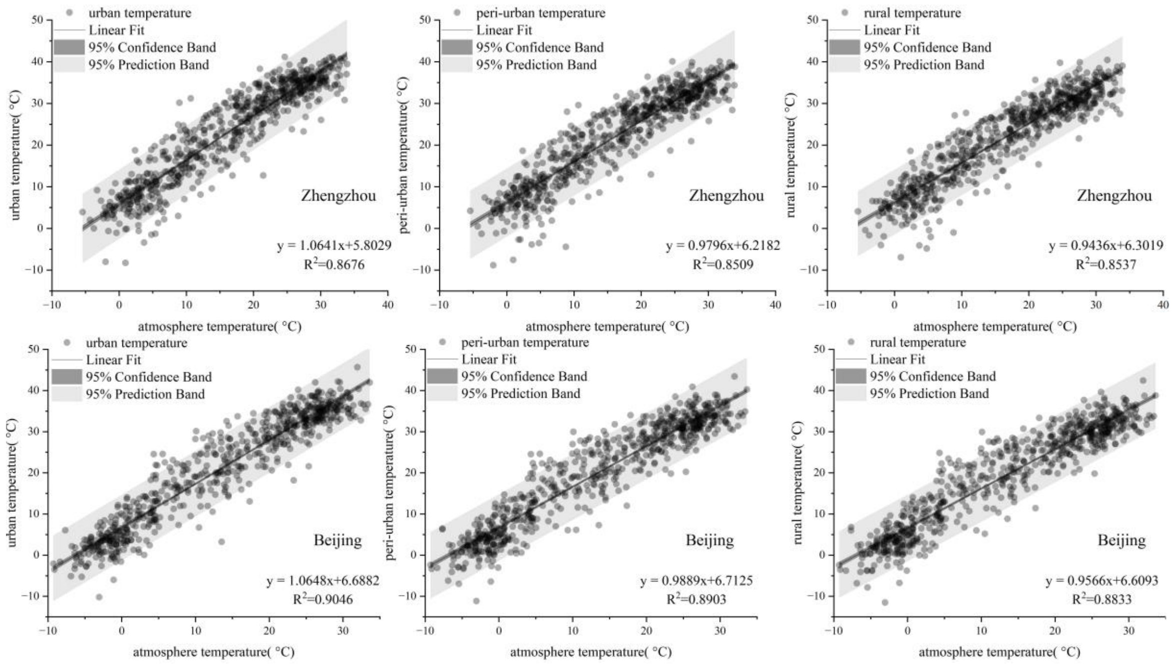

Fig. 12. Relation between urban temperature, peri-urban temperature, rural temperature and atmosphere temperature from 2000.3 to 2005.2, 2008.3 to 2013.2 and 2018.3 to 2023.2. The value of each point is the average of all the pixels in the three regions.

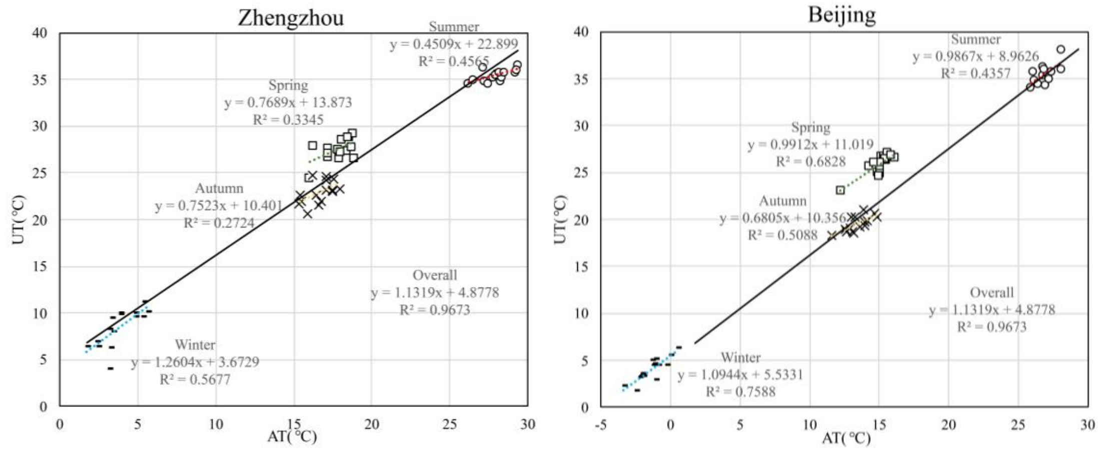

Fig. 13. LST and air temperature relation with a seasonally change in Zhengzhou and Beijing.

4 Discussion

4.1 Analysis of surface temperature changes and vegetation coverage trends in the urbanization process of Zhengzhou and Beijing

Previous research has shown that areas with denser vegetation cover have a lower heat island index compared to areas with less vegetation(Susca et al., 2011). Existing studies have used vegetation indices to assess the heat island effect and have attempted to propose methods to increase vegetation cover in order to mitigate the heat island effect (Gallo et al., 1993). This study considers the dynamic relationship between urban expansion, urban heat islands, and vegetation, calculating the impervious surface area of cities, the intensity of urban heat islands, and the vegetation index. Firstly, the expansion of urban areas shows that both Beijing and Zhengzhou have undergone significant urbanization processes in the past 20 years. This rapid urban expansion not only reflects the rapid economic development but also implies potential pressures on the local ecology and environment. Influenced by factors such as geographic location, urban layout, and green coverage, the distribution of the highest temperature month over the years in Beijing is significantly different from that in Zhengzhou, despite their similar climates. Notably, although both cities show a trend of rising temperatures, the temperature increase in Zhengzhou is more significant, which may be related to its mode of expansion during urbanization. If urban planners give insufficient consideration to the impact of the underlying surface on the thermal environment, it will largely lead to severe urban warming(Chen et al., 2006). The changes in the NDVI index of the two cities also reflect this. Beijing's NDVI value has increased over time, indicating positive efforts towards greening and ecological restoration. In contrast, the NDVI in the urban area of Zhengzhou first declined and then increased, possibly reflecting the impact of early urbanization on green spaces and subsequent restoration measures.

4.2 The pattern of urban heat island effect in Zhengzhou and Beijing

The impact of urban expansion on the urban thermal environment is significant(Zheng et al., 2023). Years of expansion, including the reconstruction within cities, will have a significant impact on the evolution of urban heat islands. Many studies have already used spatiotemporal fusion methods to study the evolution of urban heat islands (Holec et al., 2020; Meng et al., 2018), but there is still a lack of generalization on the patterns of urban heat islands. Our research established the relationship between DT and TB on a monthly average, conducting a generalized study on two cities, Beijing and Zhengzhou. The two cities exhibited different patterns, with Zhengzhou's being more complex. Zhengzhou's curve transformed from spiral to oblate, while Beijing's remained oblate. We speculate this may be related to the intensity of urban expansion in Zhengzhou. Furthermore, through the DN-DT curve, we found that the UHII distribution and trend of change in both cities were complex and showed seasonal differences. Zhengzhou's DN-DT curve showed a bimodal shape, while Beijing's was unimodal. We guess this might be related to the different crop structures in the two places. Different phenology of crops leads to different NDVIs in each season (Huemmrich et al., 1999). The unity of the DN and DT curves in both cities reflects the close relationship between NDVI and heat islands. The differences in the city models are manifested in the annual distribution and seasonal differences of UHII. Generally, the UHII is highest in summer for both cities, which is directly related to the solar radiation in summer. Therefore, strengthening the management of heat islands in summer requires great attention to the management of vegetation inside and outside the city.

4.3 Exploring Environmental Sustainability

We usually believe that the increase in impervious surfaces during urban expansion squeezes out vegetation cover, leading to a decline in NDVI both internally and externally. However, our profile study shows that urban expansion does not necessarily lead to a decline in NDVI within and around cities. During these three periods, the NDVI of Beijing's urban area showed an upward trend, while the suburbs did not show a specific trend. In contrast, Zhengzhou had its lowest NDVI during the 2010 period and its highest in the 2020 period. Zhengzhou's performance may be related to the change in its economic development policy, as in the 2020 period, Zhengzhou increased its efforts to build an environmentally friendly city and publicized the Ecological Protection and Construction Plan of Zhengzhou Metropolitan Area (2020-2035). These two cases demonstrate that even against the backdrop of rapid urban expansion, the NDVI in city centers can be improved through deliberate greening measures, reflecting the positive role of integrating green spaces into urban planning in mitigating the Urban Heat Island Intensity (UHII).

From the perspective of seasonal and time series analysis, the relationship between UHII and NDVI reveals the dynamism and complexity of urban ecosystems. This dynamism is influenced not only by urban planning and economic policies but also by natural factors such as topography and climatic conditions. Therefore, we emphasize the need for a more comprehensive perspective in urban planning and development strategies, taking into account the impact of these factors on urban ecosystems to promote the long-term sustainable development of cities.

4.4 Research contributions and limitations

The study reveals two major contributions. First, it shows that the response of Urban Heat Island (UHI) change to urbanization varies in the three phases. Second, traditional studies(Hu et al., 2020; Jamei et al., 2019) have analyzed the spatial distribution of UHI and NDVI based on spatial autocorrelation or statistical model of machine learning, and fewer studies have used profile methods in joint analyses of UHII and NDVI. We innovatively introduced clustering of the profile results, and the results suggest that crop cultivation has a significant impact on the intra-annual structure of the UHI. To some extent, this study extends current knowledge by considering the less explored application of peri-urban areas within urban heat islands. The study used Fourier curves and statistical methods to show how UHI patterns vary between two cities with different levels of development. Further insights are provided in the following detailed discussion. During the urbanization process, there is often an area with a certain proportion of impervious surface at the urban interface that experiences temperatures between urban and rural areas, and certain studies(Mehmood et al., 2022; Sismanidis et al., 2022) that include such areas as a rural component in the UHII formula may lead to low results for urban heat island effects. This study utilizes the

CCA&BGA algorithm to extract three distinct areas: the urban agglomeration, peri-urban, and rural areas. This model provides a new approach to studying the heat island phenomenon, particularly the response of urban sprawl to heat islands. Secondly, compared with the traditional statistical methods(Lu et al., 2020) and machine learning methods(Ming et al., 2023) to study the details of the heat island, the Fourier fitting curve we use can visualize the pattern of the heat island. Our research discovered that the Fourier-fitted curves for Zhengzhou spiral in 2000 and 2010 periods, then become oblate in 2020 period. Meanwhile, for Beijing, the Fourier-fitted curves remain oblate throughout all periods. Consequently, our hypothesis is that as cities continue to expand, the heat island patterns in developing cities will adopt the characteristics of those in developed cities. Furthermore, geophysical and climatic phenomena lose specificity when studied based on a singular spatial-temporal point. Therefore, this study incorporates both variables and employs a five-year observation period to more accurately capture multi-year trends and reduce errors. The limitations of the study must be acknowledged, however. The MODIS LST product in use is of low resolution and does not have the ability to capture the internal composition of the three urban areas. Yet this is a long time series study of two general urban heat island patterns, and finer imagery has less influence on these. In addition, a quantitative explanation of the various factors responsible for the marked contrasts between the two patterns is lacking, despite a comprehensive examination of urban heat island patterns at two stages of development using statistical methods and Fourier-fitted curves. Emerging interpretable neural networks may become a method for exploring causes.

5 Conclusion

In order to determine the changes in long-term UHI response due to rapid urbanization in China, this study uses MODIS data from 2000 to 2023 and employs City Clustering Algorithm and the Boundary Generation Algorithm to partition two representative cities, Beijing and Zhengzhou, according to urban, peri-urban, and rural criteria. In this study we analyze the effect on the UHI of the two cities as the urban area increases. We find that in Beijing, the heat distribution becomes more and more heterogeneous over time, while in Zhengzhou, the uniformity of the heat distribution experiences fluctuations. Further on a seasonal scale, the UHI in Beijing is relatively uniformly distributed across seasons, while Zhengzhou exhibits large variations across seasons. This suggests that the UHI patterns between the two cities may be quite different. Our further experiments corroborate this view. By Fourier fitting the curves, we found that the urban heat island effect in Beijing increased during the period of urban expansion. However, this pattern is not observed in Zhengzhou, where the heat island intensity shows a three-stage trend of decreasing and then increasing. In particular, the shape of the curve in Zhengzhou is constantly approaching that of Beijing over time, which suggests to some extent that Zhengzhou's urban pattern is converging to that of Beijing. However, the DN-DT curves we subsequently calculated indicate that the UHI response to the ecological pattern is different for the two cities. This suggests that ecological elements are not the direct cause of Zhengzhou's gradual convergence to Beijing. However, the city can still mitigate some of the adverse effects of the urban heat island by increasing vegetation and ecological planning. Subsequently, we further explored the structural dissimilarity of the two cities in terms of UHI within the city. Through the cluster analysis of the NDVI profiles, we found that the differences of NDVI between Beijing and Zhengzhou are mainly reflected in the seasonal variation, orientation variation, temporal variation, vertical variation and horizontal variation, and their patterns of change are almost opposite to those of UHII.

This investigation accentuates the distinct growth models of the two cities, incorporating peri-urban areas into the scope of urban heat island research which fills a gap in this area of study. Comparing urban spatial changes across three stages, this study reveals the differences in urban heat island patterns of cities in China with two speeds of development over the past twenty years. This study provides support for urban thermal environment planning.

Author Contributions

Conceptualization, Haibo Yang and Zhengrong Wu; methodology, Haibo Yang, Zhengrong Wu; validation, Haibo Yang and Zhengrong Wu; writing—original draft, Zhengrong Wu; writing—review and editing, Haibo Yang, Richard J. Dawson, Stuart Barr, Alistair Ford and Yunfei Li; supervision, Haibo Yang; project administration, Haibo Yang; funding acquisition, Haibo Yang. All authors have read and agreed to the published version of the manuscript.

Acknowledgments

The authors acknowledge the MODIS Products (USGS) and Globeland30 (NGCC), wish to thank Dr. Bin Zhou who provided us the CCA and BGA code. This research was supported by National Key R&D Program of China (grant number

2021YFC3200205), Henan provincial key research and development program (221111321100), and the National Natural Science Foundation of China (41101561).

Appendix

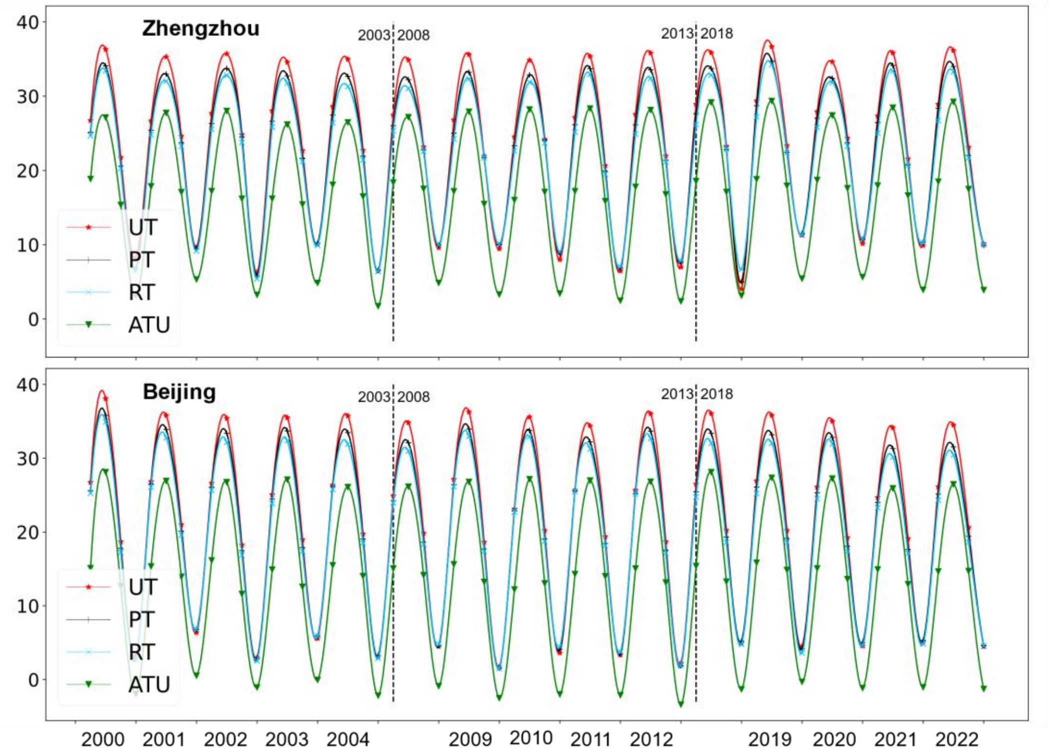

Appendix A. Quarterly changes in mean land surface temperature in urban, peri-urban and rural areas and air temperature in urban area.

Reference

Ali, G., Abbas, S., Qamer, F.M., Wong, M.S., Rasul, G., Irteza, S.M., Shahzad, N., 2021. Environmental impacts of shifts in energy, emissions, and urban heat island during the COVID-19 lockdown across Pakistan. J. Clean. Prod. 291, 125806. https://doi.org/10.1016/j.jclepro.2021.125806

Azevedo, J., Chapman, L., Muller, C., 2016. Quantifying the Daytime and Night-Time Urban Heat Island in Birmingham, UK: A Comparison of Satellite Derived

Land Surface Temperature and High Resolution Air Temperature Observations. Remote Sens. 8, 153. https://doi.org/10.3390/rs8020153

Bechtel, B., Demuzere, M., Mills, G., Zhan, W., Sismanidis, P., Small, C., Voogt, J., 2019a. SUHI analysis using Local Climate Zones—A comparison of 50 cities. Urban Clim. 28, 100451. https://doi.org/10.1016/j.uclim.2019.01.005

Bechtel, B., Demuzere, M., Mills, G., Zhan, W., Sismanidis, P., Small, C., Voogt, J., 2019b. SUHI analysis using Local Climate Zones—A comparison of 50 cities. Urban Clim. 28, 100451. https://doi.org/10.1016/j.uclim.2019.01.005

Busato, F., Lazzarin, R.M., Noro, M., 2014. Three years of study of the Urban Heat Island in Padua: Experimental results. Sustain. Cities Soc. 10, 251–258. https://doi.org/10.1016/j.scs.2013.05.001

Cai, Z., La Sorte, F.A., Chen, Y., Wu, J., 2023. The surface urban heat island effect decreases bird diversity in Chinese cities. Sci. Total Environ. 902, 166200. https://doi.org/10.1016/j.scitotenv.2023.166200

Chen, X.-L., Zhao, H.-M., Li, P.-X., Yin, Z.-Y., 2006. Remote sensing image-based analysis of the relationship between urban heat island and land use/cover changes. Remote Sens. Environ. 104, 133–146. https://doi.org/10.1016/j.rse.2005.11.016

Clinton, N., Gong, P., 2013. MODIS detected surface urban heat islands and sinks: Global locations and controls. Remote Sens. Environ. 134, 294–304. https://doi.org/10.1016/j.rse.2013.03.008

Dai, T., Qu, Z., Shi, F., 2022. Infrastructure stock in the process of urbanization in Beijing. Alex. Eng. J. 61, 3277–3291. https://doi.org/10.1016/j.aej.2021.08.060

Deilami, K., Kamruzzaman, Md., Liu, Y., 2018. Urban heat island effect: A systematic review of spatio-temporal factors, data, methods, and mitigation measures. Int. J. Appl. Earth Obs. Geoinformation 67, 30–42. https://doi.org/10.1016/j.jag.2017.12.009

Dirksen, M., 2019. Sky view factor calculations and its application in urban heat island studies. Urban Clim.

Feng, R., Wang, F., Wang, K., Wang, H., Li, L., 2021. Urban ecological land and natural-anthropogenic environment interactively drive surface urban heat island: An urban agglomeration-level study in China. Environ. Int. 157, 106857. https://doi.org/10.1016/j.envint.2021.106857

Gallo, K.P., McNab, A.L., Karl, T.R., Brown, J.F., Hood, J.J., Tarpley, J.D., 1993. The use of a vegetation index for assessment of the urban heat island effect. Remote Sens. 14, 2223–2230.

Gao, Y., Zhao, J., Han, L., 2022. Exploring the spatial heterogeneity of urban heat island effect and its relationship to block morphology with the geographically weighted regression model. Sustain. Cities Soc. 76, 103431. https://doi.org/10.1016/j.scs.2021.103431

Geng, X., Zhang, D., Li, C., Yuan, Y., Yu, Z., Wang, X., 2023. Impacts of climatic zones on urban heat island: Spatiotemporal variations, trends, and drivers in China from 2001–2020. Sustain. Cities Soc. 89, 104303. https://doi.org/10.1016/j.scs.2022.104303

Ghazanfari, S., Naseri, M., Faridani, F., Aboutorabi, H., Farid, A., 2009. Evaluating the effects of UHI on climate parameters (A case study for Mashhad, Khorrasan) 5.

He, B.-J., 2019. Towards the next generation of green building for urban heat island mitigation: Zero UHI impact building. Sustain. Cities Soc. 50, 101647. https://doi.org/10.1016/j.scs.2019.101647

Holec, J., Feranec, J., Šťastný, P., Szatmári, D., Kopecká, M., Garaj, M., 2020. Evolution and assessment of urban heat island between the years 1998 and 2016: case study of the cities Bratislava and Trnava in western Slovakia. Theor. Appl. Climatol. 141, 979–997.

Hou, H., Su, H., Liu, K., Li, X., Chen, S., Wang, W., Lin, J., 2022. Driving forces of UHI changes in China's major cities from the perspective of land surface energy balance. Sci. Total Environ. 829, 154710. https://doi.org/10.1016/j.scitotenv.2022.154710

Hu, Y., Dai, Z., Guldmann, J.-M., 2020. Modeling the impact of 2D/3D urban indicators on the urban heat island over different seasons: A boosted regression tree approach. J. Environ. Manage. 266, 110424. https://doi.org/10.1016/j.jenvman.2020.110424

Huemmrich, K.F., Black, T.A., Jarvis, P.G., McCaughey, J.H., Hall, F.G., 1999. High temporal resolution NDVI phenology from micrometeorological radiation sensors. J. Geophys. Res. Atmospheres 104, 27935–27944.

Jamei, Y., Rajagopalan, P., Sun, Q. (Chayn), 2019. Spatial structure of surface urban heat island and its relationship with vegetation and built-up areas in Melbourne, Australia. Sci. Total Environ. 659, 1335–1351. https://doi.org/10.1016/j.scitotenv.2018.12.308

Jun, C., Ban, Y., Li, S., 2014. Open access to Earth land-cover map. Nature 514, 434–434. https://doi.org/10.1038/514434c

Kim, S.W., Brown, R.D., 2021. Urban heat island (UHI) variations within a city boundary: A systematic literature review. Renew. Sustain. Energy Rev. 148, 111256. https://doi.org/10.1016/j.rser.2021.111256

Knapp, S., 2010. Urbanization causes shifts of species' trait state frequencies – a large scale analysis, in: Plant Biodiversity in Urbanized Areas: Plant Functional Traits in Space and Time, Plant Rarity and Phylogenetic Diversity. Vieweg+Teubner, Wiesbaden, pp. 13–29. https://doi.org/10.1007/978-3-8348-9626-1_2

Kolokotroni, M., Ren, X., Davies, M., Mavrogianni, A., 2012. London's urban heat island: Impact on current and future energy consumption in office buildings. Energy Build. 47, 302–311.

Lacis, A.A., Hansen, J., 1974. A parameterization for the absorption of solar radiation in the earth's atmosphere. J. Atmospheric Sci. 31, 118–133.

Li, H., Zhou, Y., Jia, G., Zhao, K., Dong, J., 2022. Quantifying the response of surface urban heat island to urbanization using the annual temperature cycle model. Geosci. Front. 13, 101141. https://doi.org/10.1016/j.gsf.2021.101141

Li, J., Song, C., Cao, L., Zhu, F., Meng, X., Wu, J., 2011. Impacts of landscape structure on surface urban heat islands: A case study of Shanghai, China. Remote

Sens. Environ. 115, 3249–3263. https://doi.org/10.1016/j.rse.2011.07.008

Li, Y., Yang, T., Zhao, G., Ma, C., Yan, Y., Xu, Y., Wang, Liangliang, Wang, Lan, 2024. A systematic review of studies involving canopy layer urban heat island: Monitoring and associated factors. Ecol. Indic. 158, 111424. https://doi.org/10.1016/j.ecolind.2023.111424

Li, Y., Zhou, B., Glockmann, M., Kropp, J.P., Rybski, D., 2021. Context sensitivity of surface urban heat island at the local and regional scales. Sustain. Cities Soc. 74, 103146. https://doi.org/10.1016/j.scs.2021.103146

Liao, Y., Shen, X., Zhou, J., Ma, J., Zhang, X., Tang, W., Chen, Y., Ding, L., Wang, Z., 2022. Surface urban heat island detected by all-weather satellite land surface temperature. Sci. Total Environ. 811, 151405. https://doi.org/10.1016/j.scitotenv.2021.151405

Lu, N., Taylor, T., Jiang, W., Jin, C., Correia, J., Leung, L.R., Wong, P.C., 2010. Climate change impacts on residential and commercial loads in the western U.S. grid. IEEE Trans. Power Syst. 25, 480–488. https://doi.org/10.1109/TPWRS.2009.2030387

Lu, Y., Wu, P., Ma, X., Yang, H., Wu, Y., 2020. Monitoring Seasonal and Diurnal Surface Urban Heat Islands Variations Using Landsat-Scale Data in Hefei, China, 2000–2017. IEEE J. Sel. Top. Appl. Earth Obs. Remote Sens. 13, 6410–6423. https://doi.org/10.1109/JSTARS.2020.3035040

Mehmood, M.S., Zafar, Z., Sajjad, M., Hussain, S., Zhai, S., Qin, Y., 2022. Time Series Analyses and Forecasting of Surface Urban Heat Island Intensity Using ARIMA Model in Punjab, Pakistan. Land 12, 142.

https://doi.org/10.3390/land12010142

Meng, Q., Zhang, L., Sun, Z., Meng, F., Wang, L., Sun, Y., 2018. Characterizing spatial and temporal trends of surface urban heat island effect in an urban main built-up area: A 12-year case study in Beijing, China. Remote Sens. Environ. 204, 826–837. https://doi.org/10.1016/j.rse.2017.09.019

Ming, Y., Liu, Y., Gu, J., Wang, J., Liu, X., 2023. Nonlinear effects of urban and industrial forms on surface urban heat island: Evidence from 162 Chinese prefecture-level cities. Sustain. Cities Soc. 89, 104350. https://doi.org/10.1016/j.scs.2022.104350

Mohammad, P., Goswami, A., 2023. Exploring different indicators for quantifying surface urban heat and cool island together: a case study over two metropolitan cities of India. Environ. Dev. Sustain. 25, 10857–10878.

Mutiibwa, D., Strachan, S., Albright, T., 2015. Land surface temperature and surface air temperature in complex terrain. IEEE J. Sel. Top. Appl. Earth Obs. Remote Sens. 8, 4762–4774. https://doi.org/10.1109/JSTARS.2015.2468594

Oke, T.R., 1982. The energetic basis of the urban heat island. Q. J. R. Meteorol. Soc. 108, 1–24. https://doi.org/10.1002/qj.49710845502

Oke, T.R., Mills, G., Christen, A., Voogt, J.A., 2017. Urban climates. Cambridge University Press.

O’Malley, C., Piroozfar, P., Farr, E.R.P., Pomponi, F., 2015. Urban Heat Island (UHI) mitigating strategies: A case-based comparative analysis. Sustain. Cities Soc. 19, 222–235. https://doi.org/10.1016/j.scs.2015.05.009

Oukawa, G.Y., Krecl, P., Targino, A.C., 2022. Fine-scale modeling of the urban heat island: A comparison of multiple linear regression and random forest approaches. Sci. Total Environ. 815, 152836. https://doi.org/10.1016/j.scitotenv.2021.152836

Saaroni, H., Amorim, J.H., Hiemstra, J.A., Pearlmutter, D., 2018. Urban Green Infrastructure as a tool for urban heat mitigation: Survey of research methodologies and findings across different climatic regions. Urban Clim. 24, 94–110. https://doi.org/10.1016/j.uclim.2018.02.001

Shahmohamadi, P., Che-Ani, A.I., Etessam, I., Maulud, K.N.A., Tawil, N.M., 2011. Healthy environment: The need to mitigate urban heat island effects on human health. Procedia Eng. 20, 61–70. https://doi.org/10.1016/j.proeng.2011.11.139

Sismanidis, P., Bechtel, B., Perry, M., Ghent, D., 2022. The Seasonality of Surface Urban Heat Islands across Climates. Remote Sens. 14, 2318. https://doi.org/10.3390/rs14102318

Stassen, C., Dommenget, D., Loveday, N., 2019. A hydrological cycle model for the Globally Resolved Energy Balance (GREB) model v1.0. Geosci. Model Dev. 12, 425–440. https://doi.org/10.5194/gmd-12-425-2019

Susca, T., Gaffin, S.R., Dell'Osso, G.R., 2011. Positive effects of vegetation: Urban heat island and green roofs. Environ. Pollut. 159, 2119–2126. https://doi.org/10.1016/j.envpol.2011.03.007

Tian, P., Li, J., Cao, L., Pu, R., Wang, Z., Zhang, H., Chen, H., Gong, H., 2021. Assessing spatiotemporal characteristics of urban heat islands from the perspective of an urban expansion and green infrastructure. Sustain. Cities Soc. 74, 103208. https://doi.org/10.1016/j.scs.2021.103208

Xia, H., Chen, Y., Song, C., Li, J., Quan, J., Zhou, G., 2022. Analysis of surface urban heat islands based on local climate zones via spatiotemporally enhanced land surface temperature. Remote Sens. Environ. 273, 112972. https://doi.org/10.1016/j.rse.2022.112972

Yan, Z., Zhou, D., Li, Y., Zhang, L., 2022. An integrated assessment on the warming effects of urbanization and agriculture in highly developed urban agglomerations of China. Sci. Total Environ. 804, 150119. https://doi.org/10.1016/j.scitotenv.2021.150119

Zheng, S., Chen, X., Liu, Y., 2023. Impact of urban renewal on urban heat island: Study of renewal processes and thermal effects. Sustain. Cities Soc. 99, 104995. https://doi.org/10.1016/j.scs.2023.104995

Zhou, D., Xiao, J., Bonafoni, S., Berger, C., Deilami, K., Zhou, Y., Frolking, S., Yao, R., Qiao, Z., Sobrino, J., 2018. Satellite Remote Sensing of Surface Urban Heat Islands: Progress, Challenges, and Perspectives. Remote Sens. 11, 48. https://doi.org/10.3390/rs11010048

Zhou, D., Zhao, S., Liu, S., Zhang, L., Zhu, C., 2014. Surface urban heat island in China's 32 major cities: Spatial patterns and drivers. Remote Sens. Environ. 152, 51–61. https://doi.org/10.1016/j.rse.2014.05.017

Zhou, Y., Zhao, H., Mao, S., Zhang, G., Jin, Y., Luo, Y., Huo, W., Pan, Z., An, P., Lun, F., 2022. Exploring surface urban heat island (SUHI) intensity and its implications based on urban 3D neighborhood metrics: An investigation of 57 Chinese cities. Sci. Total Environ. 847, 157662.

https://doi.org/10.1016/j.scitotenv.2022.157662

Zou, Z., Yan, C., Yu, L., Jiang, X., Ding, J., Qin, L., Wang, B., Qiu, G., 2021. Impacts of land use/ land cover types on interactions between urban heat island effects and heat waves. Build. Environ. 204, 108138. https://doi.org/10.1016/j.buildenv.2021.108138